# Chapter IV: Characterization and Measurement of Fiber Bragg Gratings

## 4.1 Introduction

The fiber Bragg grating (FBG) spectral characteristics is of primary importance for its proper operation. Full and accurate amplitude characterization of this device is therefore needed to apply it in DFB and DBR fiber lasers and fiber sensors. In this chapter, a detailed spectral characterization of fabricated FBGs are given. The transmission and reflection spectra are measured using two different sources namely a fiber amplifier and a semiconductor tunable laser source. The amplified spontaneous emission (ASE) from fiber amplifier is a very good broadband source, as it is able to cover the 1480 ~ 1600nm wavelength band. The tunable laser source enables more accurate measurement, as it is scanned across the wavelength range of interest, the benefit being able to obtain a larger dynamic range of the FBG spectra.

The measurement of temperature dependence of the FBG spectra is also presented in this chapter. The temperature sensitivity affects the performance of field-deployed FBG as optical devices such as tunable optical filters and optical fiber sensors [1][2]. Optical sensors based on intra-core FBGs have been used in a number of importance application areas ranging from structural monitoring to chemical sensing [3], [4], [5]. In sensing application, the FBG with low temperature sensitivity

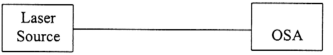


(a) Base-line measurement

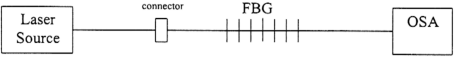


(b) Fiber grating characterisation

Figure 4.1: The set-up to determine the FBG transmission spectrum

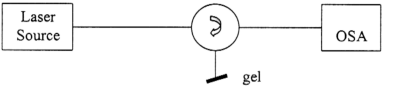


(a) Base-line measurement

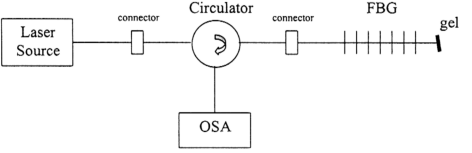


(b) Reflection spectra determination

Figure 4.2: The set-up to measure the FBG reflection spectrum

can be used as strain sensors. The sensing performance can be enhanced because the temperature dependence of the FBG is suppressed. FBG's with high temperature sensitivity can also be used as temperature sensors. Bragg wavelength shift induced by temperature variation in bare and packaged FBG's are investigated and presented in this chapter. Two different methods are used to subject the fiber Bragg grating to temperature variation i.e. using an oven and using a Peltier heat pump.

## 4.2 Measurement of transmission and reflection spectra of Bragg gratings

### 4.2.1 Transmission and reflection

A FBG is a periodic perturbation of the refractive index along the fiber length and light propagating along the fiber and encounters this perturbation where a small amount of light is reflected at each point of refractive index transition. If each of these reflections is in phase, they will add coherently and produce a large net reflection from the grating. This phase matching occurs at only one specific wavelength called the Bragg wavelength. This wavelength is given by:

$$\lambda_B = 2n_{eff}\,\Lambda \tag{4.1}$$

The bandwidth and strength of the reflection depend on the index change per period, and the overall length of the grating. The maximum reflection strength is given by

$$R_{max} = \tanh^2(\kappa L) \tag{4.2}$$

and the full width (between zeroes) of the grating reflection is given by

$$\Delta\lambda = \lambda_B^2[(\kappa L)^2 + \pi^2]^{1/2} / \pi n_{eff} L \tag{4.3}$$

where $n_{eff}$ is an effective index, $\Lambda$ is a grating period, L is grating length and $\kappa$ is the coupling coefficient (a measure of the strength of the grating).

Transmission and reflection spectra are important for characterizing a FBG. FBG characteristics such as Bragg wavelength, reflectivity, bandwidth etc. can be measured from these spectra. The set-up to measure these spectra are shown in Figure 4.1 and 4.2, respectively. First, a broadband source from a fiber amplifier is used as a high power probe source, while an optical spectrum analyzer (OSA, Anritsu MS 9710B) is used to capture and analyze the measured spectrum. The circulator functions to route the broadband ASE light to and from the FBG under test. The FBG filters the ASE light from the amplifier. The lost transmission power is actually reflected towards the direction of the incoming signal.

To start a measurement, a baseline spectrum from the amplifier is measured as in set up (a). Then, the measured spectrum is scanned in trace A of the OSA. The transmission and reflection spectra of FBG are measured using the set up in (b). The measured spectra is scanned in trace B of the OSA. The actual spectrum of the FBG is calculated by subtracting trace A from trace B. The calculated spectrum is shown in trace C of the OSA. The experiment is repeated but this time a semiconductor tunable laser source (TLS, Anritsu MG 9638A) is used as the light source, which is a narrowband source.

### 4.2.2 Fiber amplifier for characterization

Scanning with a broadband probe source is very fast compared to a narrow band source. This advantage makes the former very suitable for use in real time monitoring. The fabricated FBGs, as explained in the previous chapter are characterized using a fiber amplifier in this experiment. The measured transmission

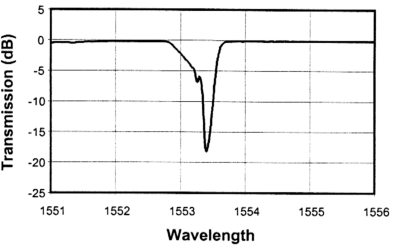
Transmission (dB)
5
0
-5
-10
-15
-20
-25
1551
1552
1553
1554
1555
1556
Wavelength

(a) FBG 1

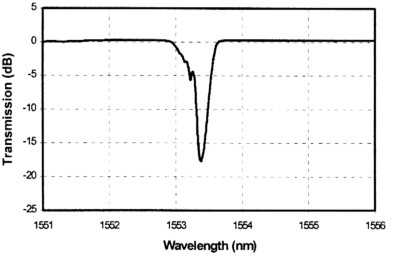
Transmission (dB)
5
0
-5
-10
-15
-20
-25
1551
1552
1553
1554
1555
1556
Wavelength (nm)

(b) FBG 2

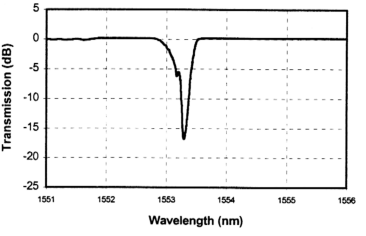


(c) FBG 3

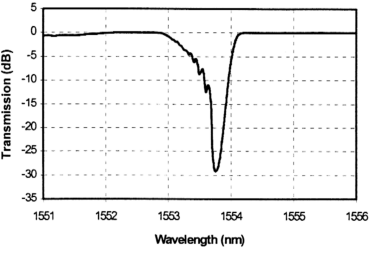


(d) FBG 4

Figure 4.3: Transmission spectrum measured by fiber amplifier (a) FBG 1 (b) FBG 2

(c) FBG 3 (d) FBG 4

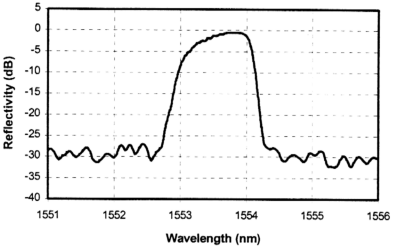
Reflectivity (dB)
5
0
-5
-10
-15
-20
-25
-30
-35
-40
1551
1552
1553
1554
1555
1556
Wavelength (nm)

(a) FBG 1

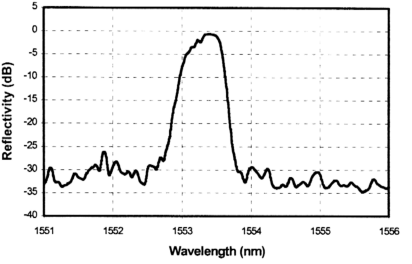
Reflectivity (dB)
5
0
-5
-10
-15
-20
-25
-30
-35
-40
1551
1552
1553
1554
1555
1556
Wavelength (nm)

(b) FBG 2

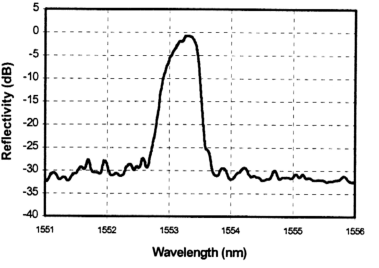


(c) FBG 3

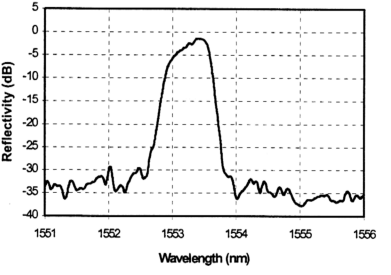


(d) FBG 4

Figure 4.4: Reflection spectrum measured by fiber amplifier (a) FBG 1

(b) FBG 2 (c) FBG 3 (d) FBG 4

| FBG | $T_d$ (dB) | Wavelength (nm) | 3dB Bandwidth (nm) |
|---|---|---|---|
| FBG 1 | 29.0 | 1553.75 | 0.12 |
| FBG 2 | 18.2 | 1553.39 | 0.08 |
| FBG 3 | 17.8 | 1553.37 | 0.11 |
| FBG 4 | 16.8 | 1553.28 | 0.08 |

Table 4.1: Transmission parameters measured using amplifier

| FBG | Peak power (dB) | Peak wavelength (nm) | 3dB $\Delta\lambda$ (nm) | 20dB $\Delta\lambda$ (nm) |
|---|---|---|---|---|
| FBG 1 | -0.57 | 1553.75 | 0.836 | 1.396 |
| FBG 2 | -1.46 | 1553.39 | 0.501 | 0.997 |
| FBG 3 | -0.72 | 1553.37 | 0.441 | 0.868 |
| FBG 4 | -0.75 | 1553.30 | 0.368 | 0.776 |

Table 4.2: Reflection parameters measured using amplifier

and reflection spectrum for these FBGs are shown in Figure 4.3 and 4.4, respectively. The transmission parameters such as transmission dip $T_d$, center wavelength, 3dB bandwidth are summarized in Table 4.1. The bandwidth was measured at + 3 dB from the transmission minima. The transmission dip is defined as a distance from the minima transmission point to full transmission level. The reflection parameters such as peak power, peak wavelength and bandwidths are shown in Table 4.2.

### 4.2.3 Tunable laser source for characterization

Special care has to be taken when measuring the transmission dip of high reflectivity FBG's because of the limited resolution of the OSA. The slit width of the spectrum analyzer is not a delta function, and there is substantial leakage from the transmitted light and affects the spectrum mostly at the dip in the grating transmission. There are several solutions to this problem, one is to use a better OSA, or two a tunable laser source may be used in conjunction with a conventional OSA, ensuring that the scanning of the laser and the OSA are synchronized with an appropriate slit width. The combined side-mode suppression, peak-to-floor separation of the TLS output and a minimum slit width of the OSA reduce the captured noise.

In this experiment, the TLS is used to measure the fabricated FBGs. The transmission and reflection spectrum measured are shown in Figure 4.5 and 4.6, respectively. Their transmission and reflection parameters are shown in Table 4.3 and 4.4, respectively.

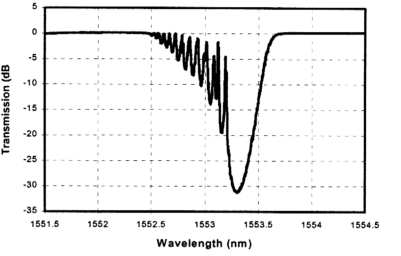
Transmission (dB
5
0
-5
-10
-15
-20
-25
-30
-35
1551.5
1552
1552.5
1553
1553.5
1554
1554.5
Wavelength (nm)

(a) FBG 1

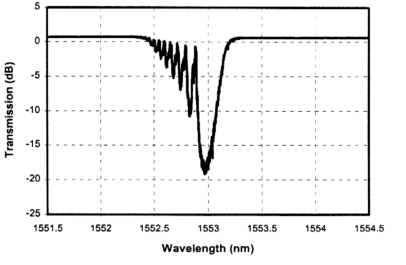
Transmission (dB)
5
0
-5
-10
-15
-20
-25
1551.5
1552
1552.5
1553
1553.5
1554
1554.5
Wavelength (nm)

(b) FBG 2

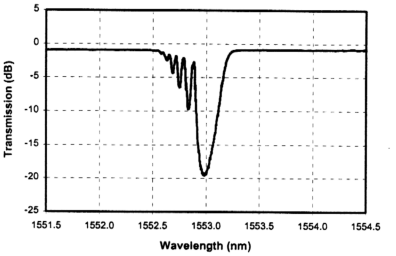


(c) FBG 3

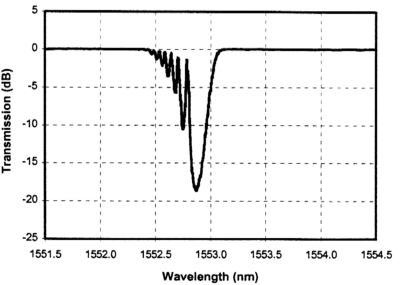


(d) FBG 4

Figure 4.5: Transmission spectrum measured by tunable laser source

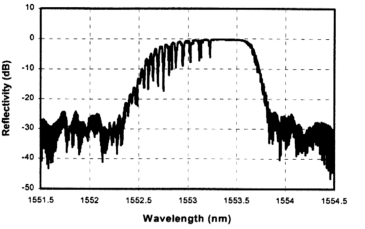
10
0
-10
-20
-30
-40
-50
Reflectivity (dB)
1551.5
1552
1552.5
1553
1553.5
1554
1554.5
Wavelength (nm)

(a) FBG 1

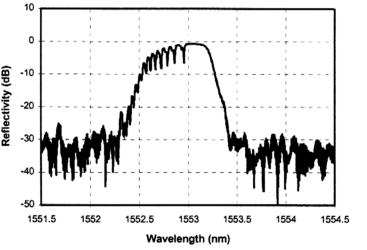
10
0
-10
-20
-30
-40
-50
Reflectivity (dB)
1551.5
1552
1552.5
1553
1553.5
1554
1554.5
Wavelength (nm)

(b) FBG 2

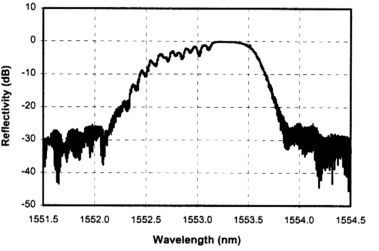


(c) FBG 3

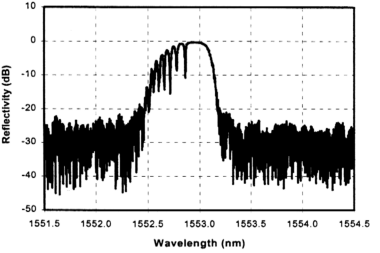


(d) FBG 4

Figure 4.6: Reflection spectrum measured by tunable laser source

| FBG | $T_d$ (dB) | Wavelength (nm) | 3dB Bandwidth (nm) |
|---|---|---|---|
| FBG 1 | 31.4 | 1553.31 | 0.13 |
| FBG 2 | 19.8 | 1552.97 | 0.10 |
| FBG 3 | 18.5 | 1552.98 | 0.12 |
| FBG 4 | 18.6 | 1552.87 | 0.10 |

Table 4.3: Transmission parameters measured using TLS

| FBG | Peak power (dB) | Peak wavelength (nm) | 3dB $\Delta\lambda$ (nm) | 20dB $\Delta\lambda$ (nm) |
|---|---|---|---|---|
| FBG 1 | -0.31 | 1553.34 | 0.964 | 1.403 |
| FBG 2 | -0.74 | 1553.04 | 0.540 | 0.993 |
| FBG 3 | -0.08 | 1553.04 | 0.501 | 0.824 |
| FBG 4 | -0.32 | 1553.96 | 0.420 | 0.785 |

Table 4.4: Reflection parameters measured using TLS

### 4.2.4 Discussion

The maximum reflectivity can be calculated by measuring the transmission dip $T_d$ in dBs. The translation from the measured transmission dip to the reflectivity is

$$\mathbf{R = 1 - 10^{-T_d/10}}. \tag{4.4}$$

A 10dB transmission dip is equivalent to a reflectivity of 90%, 20dB is 99% and so on. It is assumed that there is no additional loss in the reflected signal as compared with the transmitted signal. If the loss is known, the transmitted level must be adjusted accordingly. When the fiber amplifier is used as a probe source, the transmission dips for the fabricated FBGs are shown to be 29.0, 18.2, 17.8 and 16.8 dB. This translates to a reflectivity of 99.9, 98.5, 98.3 and 97.9%, respectively. For TLS as a probe source, the measured transmission dips are 31.4, 19.8, 18.5 and 18.6 dB. By using the same equation, these translates to a reflectivity of 99.9, 98.9, 98.6 and 98.6, respectively. The TLS shows higher reading in reflectivity compared to the fiber amplifier. It is attributed to the interplay between laser spectral width and the OSA resolution bandwidth. With broadband amplifier, a higher level noise is detected as compared to TLS.

Alternatively, the reflectivity can also be calculated from the peak of the reflected signal $R_p$. The translation from the peak reflection power to the reflectivity is

$$\mathbf{R = 10^{R_p/10}}. \tag{4.5}$$

It is assumed that there is no connector loss, circulator loss, splice loss and other additional loss in the reflected signal as compared with the transmitted signal. If the loss is known, the reflection peak is adjusted accordingly. With the fiber amplifier as a probe source, the reflection peak for the fabricated FBGs are shown to be –0.57, -1.46, -0.72 and –0.75 dB. This translates to a reflectivity of 87.7, 71.4, 84.7 and 84.1%, respectively, obtained by using equation (4.5). With the TLS as a probe source, the measured reflectivity peaks are –0.31, -0.74, -0.08 and –0.32. By using the same equation, these translate to a reflectivity of 93.1, 84.3, 98.1 and 92.9, respectively.

This calculation shows the smaller reflectivity compared to using the $T_d$ This situation is caused by the losses that are not accounted for. Calibration of reflectivity proved unreliable since the losses are not stable.

One of the advantages of the reflection spectrum is it can easily detect the very weak Bragg reflected signals. Reflections just above the noise floor of the OSA are easily displayed. When a grating is written into a fiber, a reflection peak appears which may be checked for wavelength. On the other hand, the transmission spectrum shows no change until the grating reflectivity exceeds the Fresnel reflection level of about 3 ~ 4% from the fiber end. Because of this reason, the reflection measurement is used to monitor the growth of grating at early stage for weak FBG during fabrication.

In addition to the very steep long wavelength edge, both transmission and reflection spectra have additional structures in the short wavelengths side. These side-lobes are caused by Fabry-Perot resonance [6] that are in turn caused by the induced index change being high in the middle of UV beam and low on the sides. Thus the sides form a low reflectivity Fabry-Perot interferometer. The reason why they are seen only on the short wavelengths is due to the Bragg resonance for short wavelengths for small index changes.

From the measured spectra, it is seen that the fabricated FBGs are unapodised and they have a uniform index change along the fiber. The spectra also show that the beam used and fabrication set-up is in very good alignment. A better spectrum can be obtained if the beam collimation is ensured to be perfect.

### 4.2.5 Fresnel reflection and calibration of the reflected signal

In reflection measurement, the cleaved fiber end must be index matched with index matching gel in order to avoid Fresnel reflection. It is important to implement this especially when monitoring the reflection spectrum during fabrication. In this way the growth of the narrow bandwidth reflection could be monitored when the grating is being formed. The Fresnel reflection occurs because of the difference of refractive indices of the fiber core and air. The reflectivity is about 3.6% for the fiber used. The effect of Fresnel reflection can be seen in Figure 4.7, where the use of a matching gel enables a lower floor to be seen.

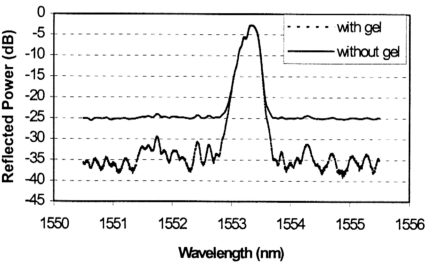


Figure 4.7: Effect of Fresnel reflection

The 3.6% Fresnel reflection can also be used to calibrate the reflected signal measured by an OSA. Figure 4.8 shows the transmission and reflection spectrum with

and without gel of one of the fabricated FBG. The base of reflection spectrum without gel indicates the Fresnel reflection and it is shown to be 0.0104 μW. Fresnel reflection was calculated to be about 3.6% for the glass/air coefficient. The reflection spectrum shows the peak of 0.0955 μW. If the base value of 0.0104 μW is equivalent to 3.6%, the peak value of 0.0955 μW should be 33.1%. However, the transmission dip of the FBG is about 1.3 dB, which is equivalent to 74.1% transmissivity. So, the maximum reflectivity of the FBG should be more than 25.9%. This shows that there are other sources of error or loss that causes the mismatch. Typically there are circulator losses, pigtail-connection losses and splice losses. Of the three the latter two are very inconsistent and vary from experiment to experiment. This factor does not allow accurate knowledge of the reflectivity without performing elaborate calibration. Hence, transmission profile is relied upon heavily.

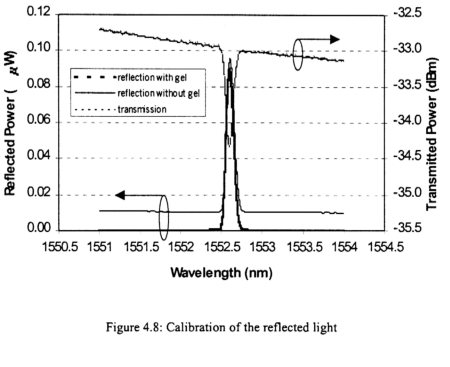


Figure 4.8: Calibration of the reflected light

## 4.3 Temperature dependence

### 4.3.1 Experimental configurations

FBGs are components used in filter and process optical signals in wavelength division multiplexed (WDM) transmission systems, dispersion compensators and sensor applications. They are rugged, all fiber components, which offer extremely sharp filter responses, narrow bandwidths and flexible design parameters. In common with competing technologies, their use in telecommunications systems employing closely spaced (high density) wavelengths has been limited by their change in center wavelength with temperature. The temperature sensitivity of a bare fiber is due to thermal expansion and thermo-optic effects.

The experimental configurations to study the Bragg wavelength drift in a bare FBG with respect to temperature variation are shown in Figure 4.9 and 4.10. These configurations utilize different methods in applying temperature onto a bare FBG. A broadband source from fiber amplifier is used as a signal source for both methods. The broadband source is selected because it enables fast scanning of the OSA, which is needed to monitor wavelength shift, effectively. The signal goes through a circulator and then is coupled into the FBG. The signal reflected from FBG is monitored using a commercial OSA (Anritsu MS 9710B).

In the first method, the temperature is accurately applied using an oven. A bare FBG is hung in the center of the oven. The applied temperature is varied between 30 ~ 125°C. In the second method, the temperature is applied using a Peltier heat pump regulated by a thermoelectric controller. The applied temperature is measured by a thermistor. The thermistor changes the applied temperature to resistance, which can be

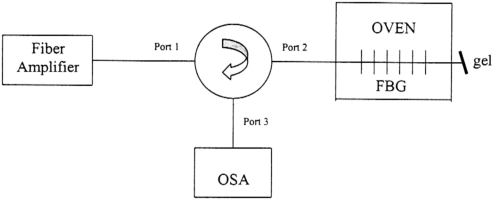


Figure 4.9: Experimental configuration of the first method

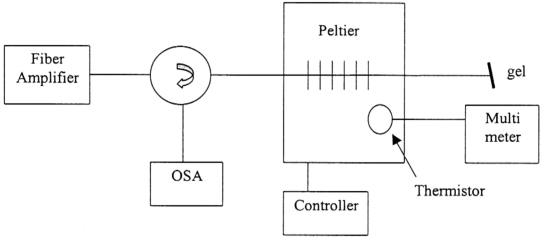


Figure 4.10: Experimental configuration for the second method

measured with a multimeter. Then, a conversion table supplied by the manufacturer is used to measure temperature from the measured resistance data. The bare FBG and thermistor are thermally bonded using a heatsink compound to a Peltier heat pump, which acts to keep the region at a constant temperature. The temperature is varied from –20 to 60 °C.

### 4.3.2 Result and discussion

The experimental results of thermal sensitivity of the bare FBG for using the first method and second method are shown in Figure 4.11 and 4.12, respectively. Both methods show that the wavelength shift has a linear response to temperature change. The experimental values of the thermal response for both methods are shown in the respective figures that are 0.010 nm/ °C, respectively. Figure 4.13 shows the reflection spectrum investigated using the first method at temperature values of 44 and 121°C. While, Figure 4.14 shows the reflection spectrum investigated using the second method at temperature values –13.1 and 27.6°C. The structure of these spectra does not change with temperature change.

Assuming a uniform grating with uniform temperature distribution, the temperature shift $\Delta\lambda$ induced by the temperature shift $\Delta T$ is given by [7], [8]

$$\Delta\lambda / \lambda = ( \alpha + \xi ) \Delta T \qquad (4.6)$$

where $\alpha$ is the thermal expansion coefficient of silica glass ( $0.55 \times 10^{-6}$ ) and $\xi$ is the thermo-optic coefficient at room temperature ( $6.9 \times 10^{-6}$ ) [9], which is about 10 times larger than the thermal expansion coefficient. This implies that the origin of the wavelength shift due to temperature variation is not thermal expansion but

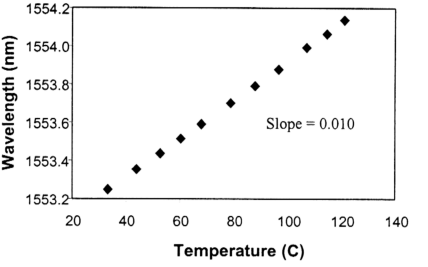


Figure 4.11: Thermal sensitivity of bare FBG using the first method

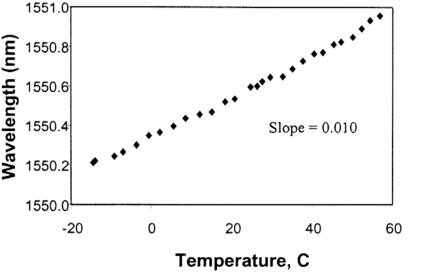


Figure 4.12: Thermal sensitivity of bare FBG using the second method

thermo-optic index change. From above equation, the theoretical value for the thermal response is calculated to be 0.012 nm/°C. As reported in the figure, both methods show the same experimental value of 0.010 nm/°C, which are consistent with the theoretical prediction value. However, a slight discrepancy between the theoretical and experimental value is observed which is probably due to the applied temperature not being distributed uniformly in the bare FBG. The induced strain during measurement is very small and can be ignored because the FBG was hung in the center of oven in the first method and it was bonded using heatsink compound to the Peltier in the second method.

Our FBG is made from a high germania boron-codoped silicate optical fiber. Pure silica and germanosilicate glass have positive thermo-optic coefficient. While pure $B_2O_3$ glass has a negative value [10]. Because the main constituent materials of the FBG are a pure silica and germanosilicate glass, the wavelength increased with temperature. If the FBG is jacketed or embedded in another substance then the sensitivity can be changed and in fact can be eliminated by the proper choice of material. Temperature sensitivity of the FBG can be suppressed by coating a negative thermo-optic coefficient material such as polymer. We also can compensate the temperature sensitivity by increasing more boron in our fiber host. Shima et al. [11] showed a high boron germanosilicate core fiber could be used to compensate temperature sensitivity in long period fiber Bragg grating. The temperature-insensitive feature is clearly desirable if the FBG is to be used as a filter or for wavelength control and stabilization of a semiconductor laser [12]. Higher thermal sensitivity also can be

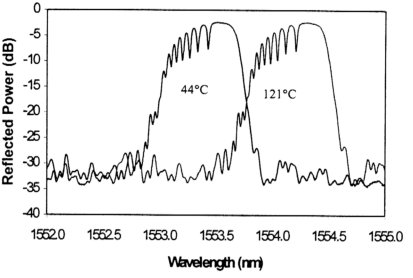


Figure 4.13: Reflection spectrum at temperature values of 44 and 121°C

from the first method

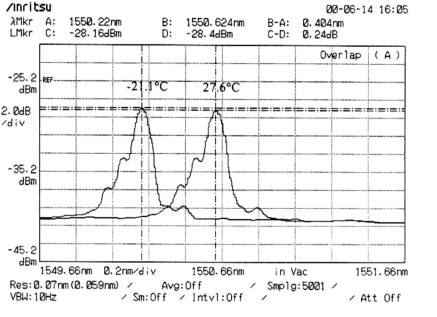


Figure 4.14: Reflection spectrum at temperature values of –21.1 and 27.6°C

from the second method

obtained if the FBG is embedded in material with a positive thermo-optic coefficient such as solder [13].

### 4.3.3 FBG packaging

Dense wavelength-division multiplexing (DWDM) network with a channel spacing as small as 0.2 nm and uneven channel spacing regimes require passive and active devices with high wavelength accuracy and stability. FBG's play an important role in various DWDM functional devices, such as FBG stabilized laser sources [12] and various WDM functional devices, since the FBG is a promising, reliable and stable in-fiber device with a low temperature coefficient of 0.01 nm/°C.

However this temperature coefficient cannot meet the temperature stability requirement of DWDM networks and other importance applications because the filter bandwidth itself may only be 0.3nm. Therefore this temperature coefficient must be reduced and packaging it proves to be a simple and cost-effective method of doing it. The packaging technique used, has 3 stages. Step one is putting a bare FBG in a U-shaped fused silica tube and fixing it with epoxy on both ends. The UV epoxy is made from mixing together a resin and a hardener. The second step is to put a heat shrink tube to cover the U-shaped fused silica tube. The last step is to put a metal sleeve as an outside package case. Special glue is put inside the metal sleeve to isolate it from outside force. The packages are shown in figure 4.15.

The temperature coefficient for each steps are measured and analyzed by the first method stated in the previous section. The wavelength shift as a function of temperature change for these packages is shown in Figure 4.16. The results show that

the temperature response reduced from 0.0101 to 0.0093 after the first packaging step, reduced again to 0.0091 in the second step. However, it increased to 0.0104 in the complete package after the third step. This packaging technique is unsuccessful to eliminate the thermal response of the bare FBG. The U-shaped fused silica tube and heat shrink tube above can reduce the thermal response by preventing the temperature from directly affecting a FBG. The metal sleeve increases the thermal response because it has a higher thermal expansion than the other materials. This situation will give rise to strain to the FBG, which in turn increases the wavelength change. It is therefore concluded that this type of packaging method is only effective to prevent FBG from breaking or damages, but it cannot effectively eliminate the thermal response of the FBG. Pic 4.1 shows a picture of the bare and packaged FBG.

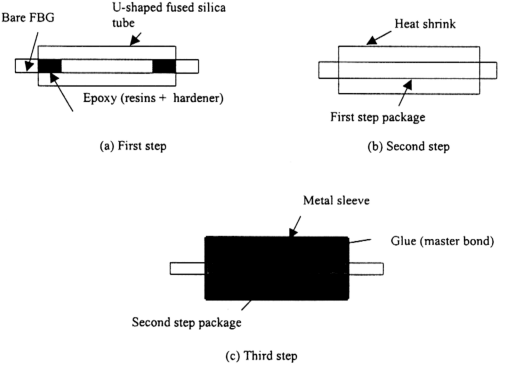


Figure 4.15: Fiber Bragg grating packaging

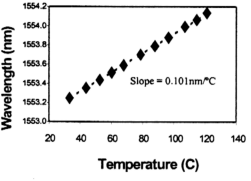


(a) Bare fiber

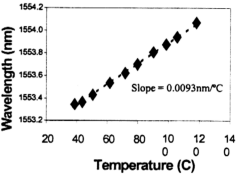


(b) First step

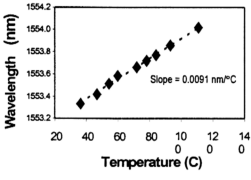


(c) Second step

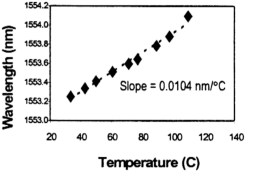


(d) Third step

Figure 4.16: The wavelength shift as a function of temperature change for packaged FBG

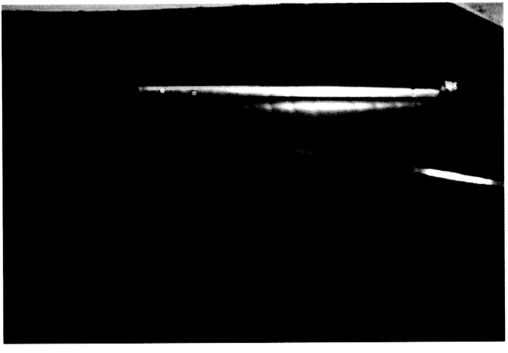

Pic.4.1: Two fabricated fibre Bragg gratings. The fibre in the foreground is a bare fibre while the one in the background is packaged in a metal cylinder as would a fibre coupler.

## 4.4 Reliability

Reliability of FBGs is essential for long-term usage in telecommunications. Thus, they have undergone numerous reliability tests in the past several years. The principle cause of its unreliability is the decay of the photoinduced index change that is greatly accelerated with temperature [14], [15]. FBG transmission and measurement recorded while ramping up the temperature have confirmed that there is thermal decay in FBGs [6]. During fabrication of a FBG, a range of energy levels is generated in the restructured glass that decay at widely different rates. The lower energy state decay more quickly and at lower temperatures. With annealing of FBG at high temperature for a short time removes the fast decay, so that at lower temperatures, the decay rate slows down. A FBG in boron-germanium co-doped fiber decay insignificantly over a

25 years period at storage temperature as high as 300K after annealing at 480K for 1 minute [16].

The issue of mechanical reliability of in-fiber FBGs has been extensively studied [17], [18]. The degradation in the strength of a fiber is due to the growth of cracks on the surface at tiny flaws. Stress concentration at these flaws propagates and causes the fiber to fail. A fiber exposed to CW 244 nm radiation is stronger than a fiber exposed to pulsed KrF radiation. With CW 244 nm radiation, the strength is almost unchanged [19], but the long-term survivability is compromised, while hydrogen loading has little influence on the breaking strength.

**References**

1. S. Huang, M.M. Ohn, M. Leblanc, R. Lee and R.M. Measures, "Fiber optic intragrating distributed strain sensor," Proc. SPIE, 2294, pp.81-92, 1994.
2. W. W. Morey and G. Meltz, W.H. Glenn, "Fiber optic Bragg grating sensors," Proc. SPIE, 1169, pp.98-107, 1989.
3. A. D. Kersey, "A review of recent developments in fiber optic sensor technology," Optic. Fiber Technol., Vol. 2, pp. 291-317, 1996.
4. G. Meltz, "Overview of fiber grating-based sensors," in Proc. SPIE Distributed and Multiplexed Sensors VI, Vol. 2838,pp.2.23, 1996.
5. A. D. Kersey, M. A. Davis, T. A. Berkoff, D. G. Bellemore, K. P. Koo and R. T. Jones, "Progress toward the development of practical fiber Bragg grating instrumentation systems," in Proc. SPIE, Fiber Optic and Laser Sensors XIV, Vol. 2839, pp. 40-64, 1996.

6. V. Mizrahi and J. E. Sipe, "Optical properties of photosensitive fiber phase gratings," J. Lightwave Tech., Vol.11, pp.1513, 1993.

7. G. Meltz and W. W. Morey, "Bragg grating formation and germanosilicate fiber photosensitivity," in Proc. SPIE Photoinduced Self-Organization Effects in Optical Fiber, F. Ouellette, Ed., Vol. 1516, pp. 185-199, 1991.

8. G. Ghosh, "Temperature dispersion of refractive indexes in some silicate fiber glasses," IEEE Photon. Tech. Lett., Vol. 6, No. 3, 1994.

9. S. Takahashi and S. Shibata, "Thermal variation of attenuation for optical fibers," J. Non-Crystalline Solids, Vol. 30, pp.359-370, 1979.

10. O. V. Mazurin, M. V. Streltsina and T. P. Shvaiko-Shavaikovskaya, "Handbook of Glass Properties," Elsevier, 1985.

11. K. Shima, K. Himeno, T. Sakai, S. Okude, A. Wada and R. Yamauchi, "A novel temperature-insensitive long period fiber grating using a boron-codoped-germanosilicate-core fiber," OFC'97 Tech. Digest, pp.347-348, 1997.

12. S. M. Lord, G. W. Switzer and M. A. Krainak, "Using fiber gratings to stabilize laser diode wavelength under modulation for atmospheric lidar transmitters," Electron. Lett. Vol. 32, pp.561-563, 1996.

13. L. Wang, G.C. Lin and C.C. Yang, "Thermal performance of a solder-coated optical fiber Bragg grating sensor," Proc. IEEE CLEO, pacific rim, pp.560, ThEE6, 1997.

14. T. Erdogan and V. Mizrahi, "Decay of UV induced fiber Bragg gratings," in Proc. Opt. Fiber Conf. OFC'94, pp. 50, 1994.

15. D. L. Williams and R. P. Smith, "Accelerated lifetime tests on UV written intracore gratings in boron germanium co-doped silica fiber," Electron. Lett., Vol. 31, No. 24, pp. 2120-2121, 1995.

16. S. R. Baker, H. N. Rourke, V. Baker and D. Godchild, "Thermal decay of fiber Bragg gratings written in boron and germanium codoped silica fiber," J. Lightwave Technol., Vol. 15, No. 8, pp. 1470-1477, 1997.

17. F. P. Kapron, H. H. Yuce, "Theory and measurement for predicting stressed fiber lifetime," Opt. Eng., Vol. 30, No. 6, pp. 700-708, 1991.

18. Y. Mitsunaga, Y. Katsuyama, H. Kobayashi and Y. Ishida, "Failure prediction for long length optical fibers based on proof testing," J. Appl. Phys., Vol. 53, No. 7, pp. 700, 1982.

19. H. G. Limberger, D. Valeras and R. P. Salathe, "Reliability aspects of fiber Bragg gratings," in Proc. of Opt. Fibre Meas. Conf., OFMC'97, pp. 18-123, 1997.